ADVANCED MATERIALS INTERFACES
Open Access
www.advmatinterfaces.de

Check for updates

Ultrastable Zn_3N_2 Thin Films via Integration of Amorphous GaN Protection Layers

*Elise Sirotti, Stefan Böhm, and Ian D. Sharp**

Zinc nitride (Zn_3N_2) is a promising semiconductor for a range of optoelectronic and energy conversion applications, offering a direct bandgap of 1.0 eV, large carrier mobilities, and abundant constituent elements. However, the material is prone to bulk oxidation in ambient environments, which has thus far impeded its practical deployment. While previous approaches have focused on stabilizing the material via integration of ZnO surface layers, these strategies introduce additional challenges regarding elevated processing temperatures and limited control of interface properties. In this study, it is shown that amorphous GaN thin films can serve as highly stable protection layers on Zn_3N_2 surfaces and can be deposited at the same growth temperature and in the same deposition system as the underlying semiconductor. The GaN-capped Zn_3N_2 structures exhibit long-term stability, surviving over 3 years of exposure to ambient conditions with no discernible alterations in composition, structure, or electrical properties. Notably, the amorphous GaN coatings can even impede Zn_3N_2 oxidation under prolonged aqueous exposure. Thus, this study offers a solution to stabilize Zn_3N_2 in ambient conditions, providing a viable pathway to its utilization in robust and high-performance electronic devices, such as thin film transistors and solar energy conversion systems.

1. Introduction

Nitride semiconductors offer a range of material properties of relevance for diverse applications, including solar energy conversion,[1] solid-state lighting,[2] and high frequency and power electronics.[3] While group III-nitrides have thus far attracted the most attention within this class of materials, group II-nitrides have increasingly emerged as interesting compound semiconductors with promising optical and electronic properties. For example, zinc nitride (Zn_3N_2) is characterized by a direct bandgap of 1.0 eV,[4] enabling efficient absorption of solar radiation, as well as high electron mobilities (approaching 400 cm^2 V^{-1} s^{-1}),[5] making it suitable as an active layer in thin-film transistor (TFT)[6] and photovoltaic devices.[7] Furthermore, it comprises only abundant elements and can be grown at considerably lower temperatures than, for example, most group IV and III–V semiconductors.

Despite these notable advantages, the severe chemical instability of Zn_3N_2, including its rapid oxidation upon exposure to ambient air, remains a major bottleneck toward its deployment in commercial applications.[8,9] In recent years, two strategies have been pursued to stabilize the material against oxidation, both of which involve the integration of ZnO layers onto the surface. In particular, Trapalis et al.[10] demonstrated that annealing of Zn_3N_2 in N_2 atmosphere at 350 °C results in stabilization of the native oxide, presumably via its improved structural quality.[10] While this approach can temporarily suppress oxidation of the underlying semiconductor, the annealing treatment requires temperatures much higher than those used for Zn_3N_2 growth, which could unintentionally alter the properties of the material,[10] especially in terms of its defect content. In an alternative approach, García Núñez et al.[11] sputter deposited a ZnO capping layer on top of Zn_3N_2.[11,12] While this strategy has been used in several investigations of Zn_3N_2-based TFTs, the influence of the deposited ZnO film on the stability of Zn_3N_2 has not been studied directly.[11–13] Overall, while both of these strategies can be used to enhance the stability of Zn_3N_2, studies of long-term durability are extremely limited.[10,14] In addition, formation of the oxide over-layer, either via annealing or deposition, could lead to some degree of oxidation of the underlying Zn_3N_2 and may restrict the ability to independently engineer the semiconductor interface characteristics.

Here, we overcome these limitations and demonstrate physically and chemically robust Zn_3N_2 thin films via deposition of amorphous GaN protection layers directly onto their surfaces. The resulting structures exhibit ultra-long-term stability, with no

E. Sirotti, S. Böhm, I. D. Sharp
Walter Schottky Institute
Technical University of Munich
85748 Garching, Germany
E-mail: sharp@wsi.tum.de

E. Sirotti, S. Böhm, I. D. Sharp
Physics Department
TUM School of Natural Sciences
Technical University of Munich
85748 Garching, Germany

The ORCID identification number(s) for the author(s) of this article can be found under https://doi.org/10.1002/admi.202400214

© 2024 The Author(s). Advanced Materials Interfaces published by Wiley-VCH GmbH. This is an open access article under the terms of the Creative Commons Attribution License, which permits use, distribution and reproduction in any medium, provided the original work is properly cited.

DOI: 10.1002/admi.202400214

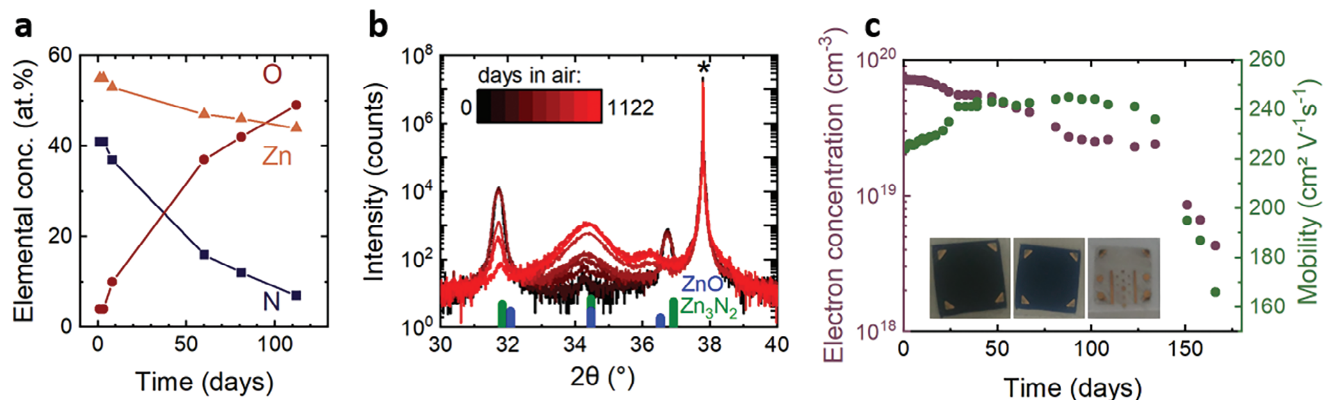

Figure 1. Oxidation of bare Zn_3N_2 thin films as a function of exposure time to ambient air. a) Elemental concentrations determined by EDX. b) HR-XRD $\theta-2\theta$ curves showing the emergence of a ZnO phase and disappearance of the Zn_3N_2 phase due to oxidation of the film. c) Hall measurements of the electron concentration (purple) and mobility (green) collected over 165 d of exposure to ambient air. (inset) Photographs of the thin film after different air exposure times: (left) as-grown Zn_3N_2, (middle) after 22 d, and (right) after 190 d of ambient exposure.

detectable compositional, optical, or electrical property changes after more than 3 years of exposure to ambient conditions. Moreover, such structures remain stable during extended immersion in liquid water. In contrast, bare Zn_3N_2 films undergo progressive oxidation and complete conversion to ZnO when exposed to ambient air for a period of a few months. The amorphous GaN layers completely suppress such oxidation and can be formed at the same growth temperature and in the same deposition system as the underlying Zn_3N_2 films, thereby enabling protection without breaking vacuum or introducing oxygen impurities. The deposited amorphous GaN films are smooth, continuous, and possess a large bandgap of over 3.2 eV, allowing complete transmission of visible light.[15] Overall, these results provide a powerful new approach to overcoming the oxidative instability of Zn_3N_2 using transparent and chemically stable protections layers, thereby opening opportunities for development of robust optical and electronic devices based on this narrow bandgap semiconductor.

2. Results and Discussion

As a starting point for understanding the protective quality of GaN capping layers, we first characterized the oxidation behavior of bare Zn_3N_2 films upon exposure to ambient air. As described in the Methods section, Zn_3N_2 films were grown by plasma-assisted molecular beam epitaxy (PA-MBE) on *a*-plane sapphire substrates. For analysis of the oxidation behavior of Zn_3N_2 during extended air exposure, a 450 nm thick film was used. **Figure 1a** shows the elemental composition of this bare Zn_3N_2 film as a function of air exposure time, as determined by energy-dispersive X-ray spectroscopy (EDX). Immediately after growth, the films are characterized by a composition of 55 at% Zn, 41 at% N, and 4 at% O. Though close to the expected Zn_3N_2 composition, the Zn:N ratio is slightly lower than the ideal value, which is likely a consequence of the known overestimation of lighter elements by EDX.[16] Upon extended exposure to air, we observe a gradual but steady decrease of the N content and concomitant increase of the O content, suggesting progressive oxidation of the bare Zn_3N_2 films. Indeed, following 112 d of air exposure, the O concentration increased from 4 at% to 49 at%. Over the same time period, the N content decreased from 41 at% to 7 at%, while the Zn content decreased from 55 at% to 44 at%. Considering the final Zn:O ratio of ≈0.9, these results suggest near-complete oxidation of Zn_3N_2 to form ZnO.

To determine the influence of oxidation on the structural properties of the films, high-resolution X-ray diffraction (HR-XRD) $\theta-2\theta$ measurements were performed as a function of ambient exposure time (Figure 1b). The diffraction pattern from the as-grown Zn_3N_2 film (black curve) is characterized by reflections at 31.7° and 36.7°, corresponding to the (222) and (100) planes, respectively, of cubic bixbyite-type Zn_3N_2, in addition to a reflection at 37.8° from the *a*-plane Al_2O_3 substrate. We note that for Zn_3N_2 layers thinner than 250 nm, only the (222) reflection is observed, indicating epitaxial growth of (111) Zn_3N_2 on *a*-plane Al_2O_3. However, for longer growth times and thicker films, the (100) reflection also appears, indicating that the upper region of the film partially loses its unique epitaxial relationship with the substrate. The data presented in Figure 1 were collected from a 450 nm thick Zn_3N_2 film and, thus, both reflections were initially present.

With increasing air exposure time, the intensities of the Zn_3N_2 reflections decrease, with the reflection at 26.7°, corresponding to the (100) oriented domains, disappearing first. Since the (100) oriented material is located on the upper surface, its more rapid decrease with exposure time is expected and confirms that oxidation propagates from the solid/air interface. In addition to the reduced intensity of Zn_3N_2 diffraction peaks with air exposure time, a broad diffraction feature emerges near 34.3°. Comparison to reference diffraction patterns reveals that both Zn_3N_2 and ZnO can possess a reflection near this position. However, considering the oxidation behavior discussed above (Figure 1a), the reflection at 34.3° can be assigned to the formation of ZnO following long-term exposure of Zn_3N_2 to air. Indeed, such oxidation results in visible changes to the optical properties of the films with increasing air exposure time. As shown in the inset of Figure 1c, the color of the film changes from black in its as-grown state, corresponding to a small bandgap of Zn_3N_2, to blue at intermediate times, and eventually to transparent, corresponding to the large bandgap of ZnO.

© 2024 The Author(s). Advanced Materials Interfaces published by Wiley-VCH GmbH
21967350, 2024, 22, Downloaded from https://advanced.onlinelibrary.wiley.com/doi/10.1002/admi.202400214, Wiley Online Library on [26/02/2025]. See the Terms and Conditions (https://onlinelibrary.wiley.com/terms-and-conditions) on Wiley Online Library for rules of use; OA articles are governed by the applicable Creative Commons License

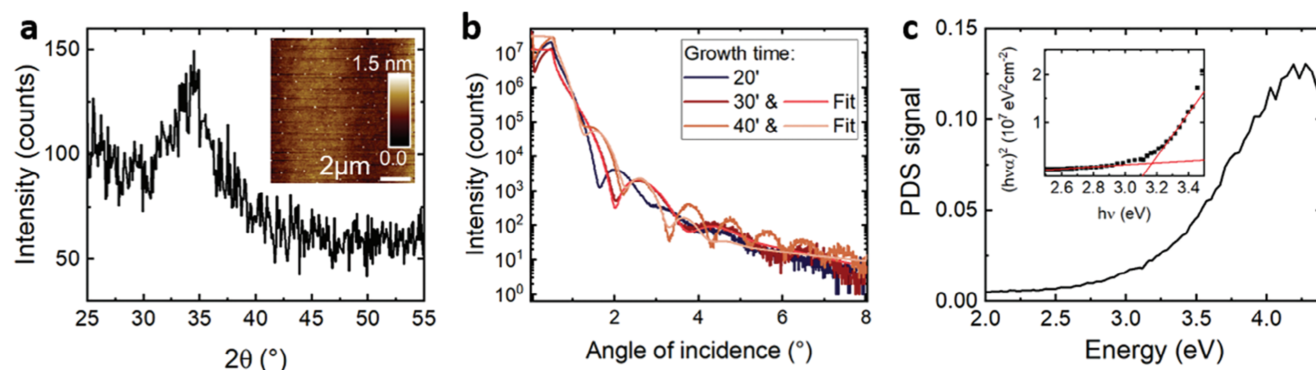

Figure 2. Characterization and optimization of amorphous GaN capping layers. a) XRD measurement of amorphous GaN on AlN. (Inset) AFM image of 8 nm thick amorphous GaN film on AlN, yielding a surface roughness of 0.5 nm and no indication of pinholes. b) XRR measurements of amorphous GaN layers grown for 20, 30, and 40 min on planar AlN substrates. Due to the large surface roughness, fitting of the 20 min growth run was not reliable. Fitting of XRR data from the 30 and 40 min deposition runs yielded thicknesses of 5 and 8 nm, respectively. The associated fits are shown in the figure and were performed with the Genetic Algorithm method offered by SmartLab Studio II (Rigaku Software). c) Optical absorption characteristics of an 8 nm thick amorphous GaN film on AlN measured with PDS. (Inset) Tauc plot analysis of the 8 nm thick amorphous GaN film.

Hall measurements of the carrier concentration and mobility within Zn_3N_2 were next performed as a function of air exposure time to determine the impact of oxidation on electrical transport characteristics (Figure 1c). As expected, all films were found to be *n*-type, with the as-grown films exhibiting a large free electron concentration of 7.3×10^{19} cm^{-3} and mobility of 225 cm^2 V^{-1} s^{-1}, which are typical for high structural quality epitaxial Zn_3N_2. Following exposure to ambient conditions, a gradual reduction of the carrier concentration is initially observed, yielding a value of 5.5×10^{19} cm^{-3} after 30 d. For exposure times beyond ≈120 d, a second regime is observed, with the carrier concentration decreasing more rapidly and eventually reaching 4.3×10^{18} cm^{-3} at 165 d, after which it was not possible to obtain reliable measurements due to the high resistivity of the film. Here, it is important to note that there is uncertainty regarding the transport path and film thickness as oxidation consumes Zn_3N_2 to produce ZnO. In addition, density differences between the two phases are expected to lead to film expansion, wherein complete oxidation can increase in the total layer thickness by a factor of ≈2, as reported by Ropero-Real et al.[17] Thus, the change in measured carrier concentration is not considered absolute, but rather represents a qualitative indicator for the effect of film oxidation with time and provides a baseline for understanding transport characteristics of protected films (see below). In contrast, the Hall mobility is less sensitive to such uncertainties since it is not a function of film thickness. As shown in Figure 1c, the mobility initially increases from 225 to 245 cm^2 V^{-1} s^{-1} during the first 30 d of ambient exposure and plateaus between 30 and 125 d, after which it decreases much more rapidly, reaching 160 cm^2 V^{-1} s^{-1} after 165 d in air. Thus, the time-dependence of both the carrier concentration and Hall mobility share a similar behavior, exhibiting more pronounced changes at long exposure times, which could indicate the point at which transport through the forming disordered ZnO phase becomes dominant.

Taken together, compositional, structural, and electrical property changes with air exposure confirm that oxidation is not self-limiting and, rather, results in near-complete conversion of the Zn_3N_2 film to ZnO. This behavior is consistent with prior findings on sputtered polycrystalline films and highlights the critical need for stabilization strategies to prevent oxidation and enable robust Zn_3N_2 for future device applications.[8] In this work, we overcome this oxidative instability via development and application of a wide bandgap GaN capping layer deposited directly onto the surface of Zn_3N_2 in the same PA-MBE growth chamber. To better facilitate morphological and optical characterization, we first characterized the GaN growth process and resulting film properties using planar and transparent AlN substrates, after which we applied the optimized coating to Zn_3N_2 surfaces. For eventual compatibility with Zn_3N_2 films, growth was performed at 150 °C, which is a significantly lower than typical temperatures used for MBE of epitaxial GaN. As a consequence, XRD of the resulting films shows a broad and weak reflection between 30° and 40° indicating that the low growth temperature yields amorphous GaN layers (**Figure 2a**). Nevertheless, XRR measurements of films grown for 30 and 40 min yield clearly defined fringes associated with planar films with thicknesses of 5 and 8 nm, respectively (Figure 2b). However, we note that fitting of XRR data from the film deposited for 20 min was unreliable due to a large surface roughness, which is consistent with island growth and an incomplete layer for this shortest deposition time. Indeed, complementary AFM measurements reveal the presence of pinholes for both the 20 and 30 min growth runs (not shown), which renders them unsuitable for application as protection layers. However, the morphology of the 8 nm thick GaN film is continuous (inset Figure 2a), with a surface roughness of 0.5 nm (compared to substrate roughness of 0.15 nm) and no indication of pinholes, suggesting its promise for encapsulation and stabilization of chemically sensitive Zn_3N_2.

In addition to being smooth and continuous, surface protection layers should ideally possess wide bandgaps that enable optical access to the underlying film. Therefore, we analyzed the optical absorption characteristics of the 8 nm thick amorphous GaN film. This was made possible by photothermal deflection spectroscopy (PDS), which is a highly sensitive technique that allows quantitative characterization of weakly absorbing transitions and ultra-thin films.[18,19] In this way, it was possible to characterize the GaN layer on a transparent substrate but with a nominally identical thickness as the protection layer deposited on top of the

 © 2024 The Author(s). Advanced Materials Interfaces published by Wiley-VCH GmbH

21967350, 2024, 22, Downloaded from https://advanced.onlinelibrary.wiley.com/doi/10.1002/admi.202400214, Wiley Online Library on [26/02/2025]. See the Terms and Conditions (https://onlinelibrary.wiley.com/terms-and-conditions) on Wiley Online Library for rules of use; OA articles are governed by the applicable Creative Commons License

ADVANCED MATERIALS INTERFACES
Open Access
www.advmatinterfaces.de

21967350, 2024, 22, Downloaded from https://advanced.onlinelibrary.wiley.com/doi/10.1002/admi.202400214, Wiley Online Library on [26/02/2025]. See the Terms and Conditions (https://onlinelibrary.wiley.com/terms-and-conditions) on Wiley Online Library for rules of use; OA articles are governed by the applicable Creative Commons License

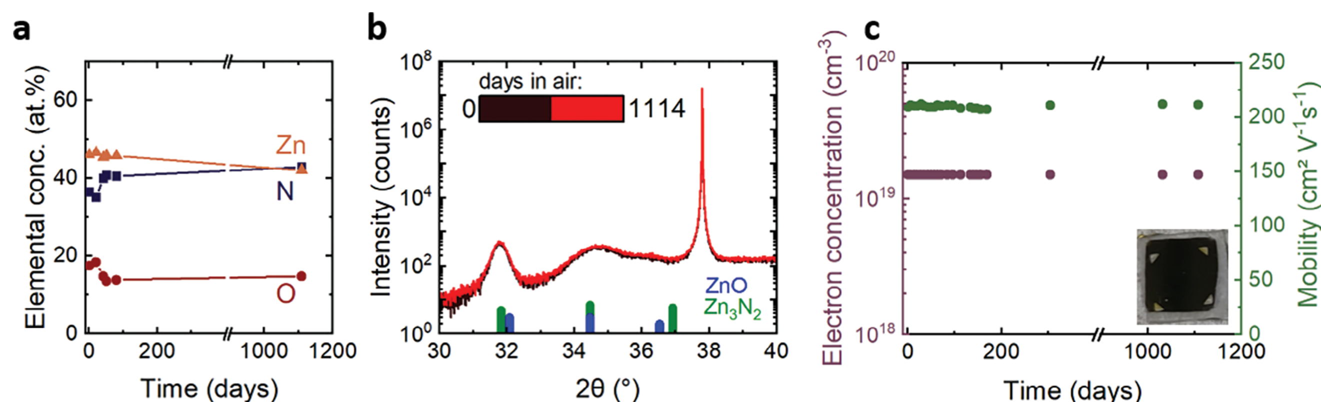

Figure 3. Stabilization of the Zn_3N_2 film with a GaN capping layer. a) Elemental concentrations determined by EDX show no indications for oxidation as a function of ambient exposure time. b) HR-XRD $\theta-2\theta$ curves from as-grown films and those after 1114 d of ambient air exposure, indicating that Zn_3N_2 is stabilized against oxidation by the amorphous GaN protection layer. c) Electron concentration (purple) and Hall mobility (green) of the GaN-capped Zn_3N_2 samples measured over 1108 d of exposure to air, with its stability highlighted by the lack of detectable differences in transport characteristics. (Inset) Photograph of the sample after 1107 d in air, indicating the stable black color of Zn_3N_2.

Zn_3N_2 films. As shown in Figure 2c, the film is characterized by a broad absorption onset in the ultraviolet range, with associated Tauc analysis indicating a bandgap of 3.2 eV. While this value is 0.2 eV lower than the known bandgap of wurzite GaN,[20] it is consistent with prior reports of amorphous GaN grown using various methods.[21] Thus, we find that these low temperature deposited amorphous GaN films offer a desirable combination of wide bandgap, continuous morphology, and thermal compatibility with Zn_3N_2 that can make them suitable as transparent protection layers. We note that attempts to characterize the electrical transport properties of the GaN film itself were not successful due to the very large resistance of the ultrathin and wide bandgap film.

Following characterization of the amorphous GaN films, we then deposited these protection layers directly onto the surfaces of Zn_3N_2 and assessed the long-term stability of the resulting structures as a function of ambient exposure time. We note that GaN deposition was performed at the same substrate temperature and in the same growth chamber immediately after Zn_3N_2 deposition, without breaking vacuum, ensuring a clean interface between the two layers. For this measurement, a 250 nm thick Zn_3N_2 film was selected to help ensure that any slow oxidation behavior could be detected against the bulk signals from the film. As shown in **Figure 3**a, EDX measurements reveal a constant composition as a function of ambient exposure time. In contrast to the bare samples (Figure 1a), no detectable oxidation is observed. Consistent with this finding, HR-XRD measurements (Figure 3b) show no evidence for the emergence of a ZnO phase, even after 1114 d of ambient exposure. Moreover, the black color of the sample, which is characteristic of the narrow direct bandgap of Zn_3N_2, remains unchanged after 1107 d in air (inset Figure 3c).

While compositional, structural, and optical measurements indicate that GaN capping layers provide long-term stability of Zn_3N_2 against oxidation in ambient conditions, we note that electrical transport characteristics can be highly sensitive to more subtle changes of the material. With this in mind, we performed Hall measurements on GaN-protected Zn_3N_2 over a period of 1108 d of exposure to ambient conditions. For this purpose, Ti/Au contacts were applied to the surface of the GaN-protected film. Despite the presence of the GaN layer, the contacts retained ohmic electrical characteristics. Remarkably, we find no change of either the electron concentration or mobility over 3 years of air exposure (Figure 3c), indicating that oxidation of Zn_3N_2 is entirely suppressed. While the measured free electron concentration of 1.5×10^{19} cm^{-3} and Hall mobility of 210 cm^2 V^{-1} s^{-1} are lower than those measured on bare as-grown Zn_3N_2, these differences arise from the difference in the initial oxygen concentrations in the films reported in Figures 1a and 3a, wherein the oxygen content is known from prior reports to influence the charge carrier concentration and mobilities of Zn_3N_2.[8,22] Measurements on two additional GaN-capped Zn_3N_2 films with different starting carrier concentrations confirm the protective quality of the coating, with no detectable changes of chemical, structural, optical, or electronic properties upon extended air exposure. Thus, we conclude that such GaN coatings can stabilize Zn_3N_2 against oxidation while preserving the properties of the active semiconductor layer. To the best of our knowledge, these samples exhibit the longest reported stability for Zn_3N_2 in air to date.[10,12,14]

To further evaluate the protective capacity of the capping layer, a bare Zn_3N_2 and a GaN-capped Zn_3N_2 sample were immersed in deionized water for 10 min and 2 h, respectively. The bare Zn_3N_2 layer dissolved partially when introduced into the water and exhibited decreased mobility and increased charge carrier concentration following water exposure. Remarkably, the GaN-capped Zn_3N_2 sample remained stable even under aqueous conditions, with no detectable change to the visible appearance, Hall mobility, or free charge carrier concentration following its much longer immersion in water. Considering that humidity in air is known to be the primary cause for oxidative degradation of Zn_3N_2,[17,23] this experiment represents an aggressive stability test, highlighting the efficacy of the developed amorphous GaN film as a protection layer for Zn_3N_2 and potentially offering opportunities for future explorations of GaN-protected Zn_3N_2 for photoelectrochemical applications.[24,25]

© 2024 The Author(s). Advanced Materials Interfaces published by Wiley-VCH GmbH

3. Conclusion

In conclusion, we have demonstrated that amorphous GaN layers grown directly on top of Zn_3N_2 are highly effective at protecting this narrow bandgap semiconductor against oxidation in ambient atmosphere, as well as in aqueous conditions. The GaN protection layers can be deposited at the same low temperature and in the same growth system as the underlying Zn_3N_2, thereby facilitating material compatibility and preventing interfacial oxidation. Comprehensive characterization of the resulting structures indicates no detectable changes to key compositional, structural, and electrical properties for at least 3 years of exposure to air. Considering that no hint of degradation is observed, this protection strategy can provide new opportunities for development of Zn_3N_2 as a high mobility, low direct bandgap, and sustainable semiconductor for various applications, including within robust TFT and solar energy harvesting devices.

4. Experimental Section

Zn_3N_2 thin films and GaN capping layers were deposited on *a*-plane sapphire using a Riber 32 PA-MBE system equipped with Zn and Ga effusion cells, as well as a radio frequency (rf) plasma source that was supplied with high purity Ar and N_2 via mass flow controllers. For reference, additional GaN layers were also grown on (0001) AlN substrates. All films were deposited at a substrate temperature of 150 °C following cleaning and conditioning via 10 min of nitrogen plasma exposure, after which film growth was initiated. The encapsulated Zn_3N_2 layers were ≈250 nm thick and have an additional ≈8 nm thick GaN capping layer grown in the same PA-MBE chamber immediately after Zn_3N_2 deposition. For reference, bare Zn_3N_2 films with a thickness of ≈450 nm was deposited under identical N_2 flow, plasma power, Zn-cell and substrate temperatures but for longer times and without inclusion of the capping layer. Following growth, both types of samples (bare and GaN-capped) were stored together under identical conditions, in ambient laboratory air, and their properties were studied as a function of exposure time. During the course of this extended exposure, the temperature and relative humidity were continuously monitored, and varied naturally between 21–27 °C and 20–70%, respectively.

Structural characterization was performed using HR-XRD with a Rigaku SmartLab 3 kW system equipped with a Cu $K_{\alpha 1}$ source and a Ge(220) × 2 monochromator in a parallel beam geometry. After coarse sample surface alignment, precision alignment was performed via rocking curve measurements of the (11-20) sapphire substrate reflection, thereby enabling quantitative evaluation of changing film diffraction intensities as a function of air exposure time. To determine the Zn_3N_2 layer thickness a stylus profilometer was used. To determine the GaN layer thicknesses, XRR measurements were performed using the same Rigaku SmartLab system. Sample morphologies and GaN film coverages were assessed using a Veeco MultiMode AFM in tapping mode. Film compositions were characterized via EDX using a Bruker XFlash6130 detector mounted on a Zeiss EVO MA10 scanning electron microscope (SEM) operated with an electron beam energy of 5 keV. The collected spectra were quantified using the Phi(rho,z) method and deconvolution function SeriesFit. Optical absorption spectra were collected with a home-built PDS setup. The sample was immersed in perfluorohexane (C_6F_{14}) within a quartz cuvette, which was placed on a translation and rotation stage for optical alignment, and was illuminated at normal incidence with focused monochromatic light obtained from a Xenon lamp (OSRAM Xenon Short Arc XBO/150 W) passed through a monochromator (Oriel, 1200 lines per mm grating). The incident light was chopped at 9 Hz. The absorption was probed using a HeNe laser (2 mW, 632.8 nm, HNL020L, Thorlabs) directed parallel to the sample surface, with deflection arising due to heat transfer from the absorbing sample and thermal lensing in the perfluorohexane. A position-sensitive detector (2-quadrant photodiode) was used to track the deflected probe laser beam. The detector and the chopper were connected to a lock-in amplifier (Princeton Applied Research Model 5210), which was used to isolate and amplify the signal at the modulation frequency. Room temperature Hall measurements were conducted with an EGK, Hem-2000 Hall effect measurement system with an applied magnetic field of ±0.58 T. All measurements were performed using ohmic Au contacts fabricated by evaporating 80 nm Au onto a 20 nm Ti adhesion layer using shadow masks in the van der Pauw geometry.

Acknowledgements

This project has received funding from the European Research Council (ERC) under the European Union's Horizon 2020 research and innovation programme (grant agreement No. 864234), as well as from the Federal Ministry of Education and Research (BMBF, Germany) project number 033RC021B within the CO2-WIN initiative and from TUM.Solar in the context of the Bavarian Collaborative Research Project Solar Technologies Go Hybrid (SolTech).

Conflict of Interest

The authors declare no conflict of interest.

Data Availability Statement

The data that support the findings of this study are available from the corresponding author upon reasonable request.

Keywords

electronic transport, gallium nitride, hall effect, oxidation, protection layer, zinc nitride

Received: March 10, 2024
Revised: June 11, 2024
Published online: June 22, 2024

[1] A. Zakutayev, C. M. Caskey, A. N. Fioretti, D. S. Ginley, J. Vidal, V. Stevanovic, E. Tea, S. Lany, *J. Phys. Chem. Lett.* **2014**, *5*, 1117.
[2] R.-J. X. Le Wang, T. Suehiro, T. Takeda, N. Hirosaki, *Chem. Rev.* **2018**, *118*, 1951.
[3] F. Roccaforte, M. Leszczynski, *Nitride Semiconductor Technology: Power Electronics and Optoelectronic Devices*, Wiley-VCH, Weinheim, Germany **2020**.
[4] S.-H. Yoo, A. Walsh, D. O. Scanlon, A. Soon, *RSC Adv.* **2014**, *4*, 3306.
[5] P. Wu, T. Tiedje, H. Alimohammadi, V. Bahrami-Yekta, M. Masnadi-Shirazi, C. Wang, *Semicond. Sci. Technol.* **2016**, *31*, 10LT01.
[6] K. Li, A. Shimizu, X. He, K. Ide, K. Hanzawa, K. Matsuzaki, T. Katase, H. Hiramatsu, H. Hosono, Q. Zhang, T. Kamiya, *ACS Appl. Electron. Mater.* **2022**, *4*, 2026.
[7] C.-T. Li, H.-Y. Chang, Y.-Y. Li, Y.-J. Huang, Y.-L. Tsai, R. Vittal, Y.-J. Sheng, K.-C. Ho, *ACS Appl. Mater. Interfaces* **2015**, *7*, 28254.
[8] C. G. Núñez, J. L. Pau, M. J. Hernández, M. Cervera, E. Ruíz, J. Piqueras, *Thin Solid Films* **2012**, *522*, 208.
[9] A. Trapalis, J. Heffernan, I. Farrer, J. Sharman, A. Kean, *J. Appl. Phys.* **2016**, *120*, 205102.
[10] A. Trapalis, I. Farrer, K. Kennedy, A. Kean, J. Sharman, J. Heffernan, *AIP Adv.* **2020**, *10*, 469.

© 2024 The Author(s). Advanced Materials Interfaces published by Wiley-VCH GmbH

21967350, 2024, 22, Downloaded from https://advanced.onlinelibrary.wiley.com/doi/10.1002/admi.202400214, Wiley Online Library on [26/02/2025]. See the Terms and Conditions (https://onlinelibrary.wiley.com/terms-and-conditions) on Wiley Online Library for rules of use; OA articles are governed by the applicable Creative Commons License

[11] C. García Núñez, J. L. Pau, M. J. Hernández, M. Cervera, J. Piqueras, *Appl. Phys. Lett.* **2011**, *99*, 76101.
[12] C. García Núñez, J. L. Pau, E. Ruíz, J. Piqueras, *Appl. Phys. Lett.* **2012**, *101*, 1117.
[13] M. A. Dominguez, J. L. Pau, M. Gómez-Castaño, J. A. Luna-Lopez, P. Rosales, *Thin Solid Films* **2016**, *619*, 261.
[14] M. A. Dominguez, J. L. Pau, A. Redondo-Cubero, *IEEE Trans. Electron Devices* **2018**, *65*, 1014.
[15] R. C. Powell, N.-E. Lee, Y.-W. Kim, J. E. Greene, *J. Appl. Phys.* **1993**, *73*, 189.
[16] B. Shirley, E. Jarochowska, *Facies* **2022**, *68*, 181.
[17] A. Ropero-Real, N. Gordillo, J. L. Pau, A. Redondo-Cubero, *ACS Appl. Mater. Interfaces* **2021**, *13*, 56655.
[18] W. B. Jackson, N. M. Amer, A. C. Boccara, D. Fournier, *Appl. Opt.* **1981**, *20*, 1333.
[19] O. Bienek, B. Fuchs, M. Kuhl, T. Rieth, J. Kühne, L. I. Wagner, L. M. Todenhagen, L. Wolz, A. Henning, I. D. Sharp, *ACS Photonics* **2023**, *10*, 3985.
[20] H. P. Maruska, J. J. Tietjen, *Appl. Phys. Lett.* **1969**, *15*, 327.
[21] T. Hariu, T. Usuba, H. Adachi, Y. Shibata, *Appl. Phys. Lett.* **1978**, *32*, 252.
[22] X. Cao, A. Sato, Y. Ninomiya, N. Yamada, *J. Phys. Chem.* **2015**, *119*, 5327.
[23] M. Gómez-Castaño, A. Redondo-Cubero, L. Vázquez, J. L. Pau, *ACS Appl. Mater. Interfaces* **2016**, *8*, 29163.
[24] M. Zhong, T. Hisatomi, Y. Sasaki, S. Suzuki, K. Teshima, M. Nakabayashi, N. Shibata, H. Nishiyama, M. Katayama, T. Yamada, K. Domen, *Angew. Chem.* **2017**, *129*, 4817.
[25] G. Zeng, T. A. Pham, S. Vanka, G. Liu, C. Song, J. K. Cooper, Z. Mi, T. Ogitsu, F. M. Toma, *Nat. Mater.* **2021**, *20*, 1130.

© 2024 The Author(s). Advanced Materials Interfaces published by Wiley-VCH GmbH

21967350, 2024, 22, Downloaded from https://advanced.onlinelibrary.wiley.com/doi/10.1002/admi.202400214, Wiley Online Library on [26/02/2025]. See the Terms and Conditions (https://onlinelibrary.wiley.com/terms-and-conditions) on Wiley Online Library for rules of use; OA articles are governed by the applicable Creative Commons License